Effects of channel geometry on buoyancy-driven mixing

Yannick Hallez[a] and Jacques Magnaudet[b]
Institut de Mécanique des Fluides de Toulouse, UMR CNRS/INPT/UPS 5502, Allée du Professeur Camille Soula, 31400 Toulouse, France

(Received 17 September 2007; accepted 3 April 2008; published online 12 May 2008)

The evolution of the concentration and flow fields resulting from the gravitational mixing of two interpenetrating miscible fluids placed in a tilted tube or channel is studied by using direct numerical simulation. Three-dimensional (3D) geometries, including a cylindrical tube and a square channel, are considered as well as a purely two-dimensional (2D) channel. Striking differences between the 2D and 3D geometries are observed during the long-time evolution of the flow. We show that these differences are due to those existing between the 2D and 3D dynamics of the vorticity field. More precisely, in two dimensions, the strong coherence and long persistence of vortices enable them to periodically cut the channels of pure fluid that feed the front. In contrast, in 3D geometries, the weaker coherence of the vortical motions makes the segregational effect due to the transverse component of buoyancy strong enough to preserve a fluid channel near the front of each current. This results in three different regimes for the front velocity (depending on the tilt angle), which is in agreement with the results of a recent experimental investigation. The evolution of the front topology and the relation between the front velocity and the concentration jump across the front are investigated in planar and cylindrical geometries and highlight the differences between 2D and 3D mixing dynamics. © *2008 American Institute of Physics*. [DOI: 10.1063/1.2918379]

I. INTRODUCTION

The gravitational mixing of two miscible fluids with different densities in a pipe or a channel of arbitrary inclination with respect to the vertical provides a good model for a wide variety of situations of practical interest. For instance, it mimics flow conditions encountered in liquid-liquid separators or in oil wells but is also to some extent a relevant model for the propagation of fires in buildings. It has also well-known applications in geophysical flows such as avalanches or turbidity currents, to mention just a few. When the pipe or channel axis is almost horizontal, the problem tends toward that of gravity currents in a confined geometry. In contrast, a Rayleigh–Taylor configuration constrained by wall effects is recovered when the flow axis is vertical. The present paper describes some results obtained during an extensive numerical investigation of this class of problems. We are particularly interested in evaluating the influence of the channel geometry, as there are indications that it may induce important differences in the dynamics of the mixing. We also wish to evaluate if, under some circumstances, a two-dimensional approximation is able to correctly predict the actual flow evolution. The initial motivation of this study was provided by the thorough experimental investigation performed by Séon *et al.*[1–4] in a tilted cylindrical tube. This is why we shall pay a peculiar attention to this configuration in what follows.

Most theoretical and computational work about gravity currents on a horizontal plane has been achieved in two-dimensional (2D) configurations, e.g., theoretical predictions[5,6] and numerical simulations.[7,8] In contrast, experiments generally use three-dimensional (3D) channels with a rectangular cross section[9,10]. Recently, some computational studies also started to consider 3D gravity currents[11,12] and highlighted differences with 2D simulations. Especially, some of these investigations[12–14] pointed out that 2D simulations correctly predict the evolution of gravity/density currents during their initial acceleration phase as well as during the next phase within which the velocity of the front remains constant (usually termed as the slumping phase), whereas 2D models tend to underpredict the front velocity during later stages. This difference seems to be related to the tendency for 2D currents to create more intense coherent vortices than their 3D counterparts, due to the possibility for vortices to be stretched and tilted in a 3D flow. According to Ref. 12, vortices stand quite far from the head of the current during the slumping stage and thus do not influence significantly its behavior and velocity. In contrast, during the viscous stage, they tend to stand closer to the head and are in position to influence its evolution. Since 2D vortices are stronger than their 3D counterpart, so is their influence. As vortex cores are located in zones of low dynamic pressure, 2D vortices generate intense low-pressure zones behind the head of the current and thus slow it down. While somewhat different, a related explanation for the discrepancies between 2D and 3D predictions was proposed in Ref. 14 in the case of density currents. These authors noticed that in 2D flows, the vertical mixing generated by the strong coherent vortices involves a smaller viscous dissipation than in 3D flows, whereas the energy loss associated with particle settling is larger in the former case. In summary, both studies suggest that 3D effects cannot be ignored in the long-time dynamics of gravity/density currents, the key point being the structural differences between 2D and 3D vorticity dynamics. Much fewer investigations have been devoted to the case

[a]Electronic mail: hallez@imft.fr.
[b]Electronic mail: magnau@imft.fr.

 © 2008 American Institute of Physics

Downloaded 11 Feb 2011 to 194.167.203.33. Redistribution subject to AIP license or copyright; see http://pof.aip.org/about/rights_and_permissions

where the current takes place on a nonzero slope, a situation in which the longitudinal component of buoyancy provides a continuous forcing to the system. The case of a current fed by a continuous source and that of a sudden release of heavy fluid were both considered. Most of these studies focused on the characteristic time at which the slope starts to influence the front dynamics or the further evolution of the front velocity and size of the head with the slope (e.g., Refs. 15 and 16). In particular, the current Froude number was found to exhibit little dependence on the slope.[10]

The situation is drastically different in a confined geometry such as a tube or a closed channel. More precisely, the recent experiments performed by Séon *et al.*[1,3] in a cylindrical tube revealed the existence of three different regimes, depending on the tilt angle θ. In the range of density contrast, fluid viscosity, and tube diameter they explored, they found that for θ in between 0° (vertical tube) and 60°, approximately, Kelvin–Helmholtz instabilities grow along the interface between the two fluids, enabling a strong transverse mixing. When the tilt angle was set in between 60° and 80°, approximately, the transverse component of buoyancy started to act, increasing segregation effects. In this case, some pure light (heavy) fluid remained stuck in the head of the ascending (descending) current and the velocity of the front reached a plateau value close to $0.7V_t$, where $V_t \sim \sqrt{Atgd}$ is the characteristic velocity of the front resulting from a balance between buoyancy and inertia forces, where $\mathrm{At}=(\rho_2-\rho_1)/(\rho_2+\rho_1)$ is the Atwood number, g is the gravity, and d is the tube diameter (the density of the heavy and light fluids are ρ_2 and ρ_1, respectively). This situation where a channel of pure light fluid rises in a pure heavy fluid is qualitatively similar to the case of large air bubbles rising in tubes filled with liquid. Finally, for quasi-horizontal tubes, no significant mixing was noticed and, after the initial stage during which the above scaling holds, potential energy was observed to be gradually dissipated by viscosity, as in the case of horizontal unconfined gravity currents.

In the present paper, we make use of the complementary approach provided by direct numerical simulation to shed additional light on the role of confinement and channel geometry on the flow evolution and mixing characteristics. For instance, in a certain range of tilt angles, several experimental runs in Ref. 3 exhibited flows with vortices located far from the head of each current, even in the late stages of the evolution. This structure of the vortex field resembles that numerically observed in Ref. 12 during the slumping stage of horizontal gravity currents, a stage for which the 2D approximation proved to provide a reliable description. Therefore, we can wonder whether in a certain range of parameters, the main features of the gravitational mixing can be recovered with a 2D model. Finally, for a certain "level" of lateral confinement, it is also of interest to investigate whether or not the precise shape of the channel cross section has a significant influence on the flow evolution. To reach the above goals, we carried out a series of computations in four different geometries, namely, a purely 2D configuration, a 3D cylindrical tube, a square duct with a no-slip condition on all four walls, and a 3D periodic channel that is identical to the previous square duct, except in that the two lateral walls are submitted to a periodic condition instead of a no-slip one (the latter configuration is that used in available 3D simulations of gravity currents[11–14]). After we briefly present and validate the numerical tool we use, we devote the rest of this paper to an analysis of the evolution of the flow and concentration fields in these various geometrical configurations.

II. NUMERICAL APPROACH

Let C be the local volume fraction of the heavy fluid 2. The mixture density is then

$$\rho = C\rho_2 + (1-C)\rho_1. \tag{1}$$

We assume the molecular diffusivity of the binary system to be negligibly small, which implies[17]

$$\nabla \cdot \mathbf{U} = 0. \tag{2}$$

Therefore, combining Eq. (1) with the mass balance of the mixture implies the governing equation for C to be

$$\frac{\partial C}{\partial t} + \nabla \cdot (C\mathbf{U}) = 0, \tag{3}$$

where $\mathbf{U}$ denotes the mass-averaged velocity.

The mixture is assumed to behave as a Newtonian fluid with a dynamic viscosity μ independent of C. Therefore, the momentum balance can be expressed as

$$\frac{\partial \mathbf{U}}{\partial t} + \mathbf{U}\cdot\nabla\mathbf{U} = \mathbf{g} - \frac{1}{\rho}\nabla P + \nu\nabla\cdot(\nabla\mathbf{U} + {}^T\nabla\mathbf{U}), \tag{4}$$

where $\nu=\mu/\rho$ is the (variable) kinematic viscosity of the mixture. The Navier–Stokes system (2)–(4) with ρ given by Eq. (1) is solved by using the JADIM code developed in our group. The numerical approach is briefly summarized here; more details can be found in Ref. 18. First of all, the volume concentration (3) is solved by using a flux corrected transport (FCT) scheme. For this purpose, the equation is split into three successive substeps, one along each grid direction. Within each substep, a Zalesak scheme[19] is used to discretize the spatial flux of the left-hand side. This scheme combines the use of a low-order (here first-order) and a high-order (here fourth-order) spatial discretization to preserve positivity and monotonicity of the solution and to ensure second-order spatial accuracy. It is worth pointing out that other numerical schemes, such as the fifth-order weighted essentially non-oscillating (WENO) scheme, were tried as well on several reference test cases. Zalesak's FCT scheme emerged as the one that yields the most accurate solution in most situations and was thus selected for the rest of our investigation. Equation (4) is discretized on a staggered nonuniform grid using a finite-volume formulation; all spatial derivatives are expressed through second-order centered schemes. Time advancement is achieved through a third-order Runge–Kutta algorithm for advective and source terms, whereas the viscous term is advanced semi-implicitly through a Crank–Nicholson algorithm. This advancement step produces a velocity field $\mathbf{U}^*$. Then, condition (2) is satisfied by using a variable-density projection technique. More precisely, we solve the pseudo-Poisson equation

Downloaded 11 Feb 2011 to 194.167.203.33. Redistribution subject to AIP license or copyright; see http://pof.aip.org/about/rights_and_permissions

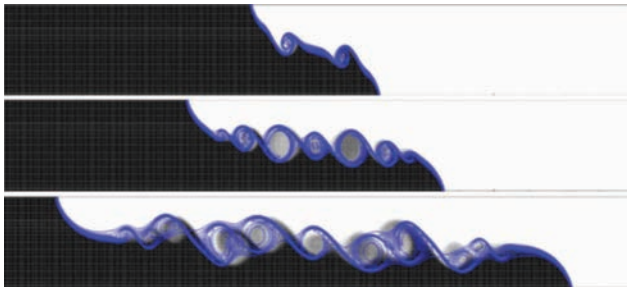

FIG. 1. (Color online) Comparison of two computations of a 2D horizontal lock-exchange flow for Re=4000 and $\rho_1/\rho_2=0.998$ (free-slip conditions are used on the upper and lower walls). Grayscale image: Results from Ref. 8. Solid lines: Isodensity contours for present results.

$$\nabla \cdot \left(\frac{1}{\rho^{n+1}} \nabla \Phi^{n+1} \right) = \frac{1}{\Delta t} \nabla \cdot \mathbf{U}^*, \tag{5}$$

where ρ^{n+1} is the mixture density obtained after solving Eq. (3) during the $(n+1)$th time step, Φ^{n+1} is the pressure increment, and Δt is the current time step. The corresponding linear system is solved with a Jacobi preconditioned conjugate gradient technique available in the ITPACK or PETSc libraries.

III. PRELIMINARY VALIDATION

Thorough validations of the JADIM code in constant-density flows may be found in previous papers (see, e.g., Ref. 20 and references therein). We therefore focus on two variable-density situations relevant to the present study. As a first example, Fig. 1 compares the results we obtained on a 2D full-depth lock-exchange flow with those recently published by Birman *et al.*[8] on the same configuration.

The two series of snapshots indicate very similar behaviors. In particular the location of the front predicted by the two computations is exactly the same at all times. The vortices produced at the interface are also almost identical. Only a slight shift of some of these vortices can be noticed. This difference is probably attributable to a Schmidt number effect, since the two fluids are almost immiscible in our computation (see below), while the Schmidt number is unity in Ref. 8 (the Schmidt number is the ratio of the kinematic viscosity to the binary molecular diffusion coefficient).

Our second validation is directly related to the aforementioned experiments of Séon *et al.*,[3] to which the reader is referred for details. We adjust the flow parameters so as to fit the experimental conditions. Therefore, the Atwood number is set to At=0.004 (as in the rest of this paper, unless specified otherwise), whereas the Reynolds number $\mathrm{Re}=g'^{1/2}d^{3/2}/\nu$, where $g'=g(\rho_2-\rho_1)/\rho_1$ is set to Re=790. The experimental Schmidt number is about 10^3. In the computations we let it be theoretically infinite. In practice, this means that the physical cutoff lengthscale imposed by the molecular diffusivity is replaced by an artificial cutoff lengthscale of the order of the grid cell size, say, Δ. Indeed, when two fluid elements, one of fluid 1 the other of fluid 2, enter a control volume of $O(\Delta^3)$, they immediately mix and cannot separate any more. Therefore, there is a small but finite effective numerical diffusivity which was estimated through specific tests. The corresponding numerical Schmidt number was found to be of $O(10^3)$. The computational domain is a cylindrical tube of diameter d and length $32d$. The grid is axisymmetric with 512 cells along the tube axis, 32 cells over one tube radius, and 64 cells along the azimuthal direction (the grid is refined near the wall in the radial direction so as to capture near-wall gradients, see Fig. 2). Some computations were also run using 64 cells over one tube radius but this produced only marginal changes in the solution.

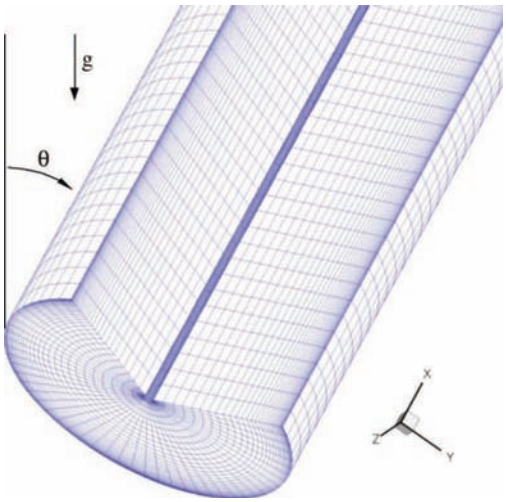

FIG. 2. (Color online) Cylindrical grid and definition of the tilt angle.

As long as the front of the current is not close to an endwall (which is satisfied throughout all computations), the tube length has no effect on the instantaneous dynamics of the flow. However, this length directly determines the total time over which the flow evolution can be observed before it is influenced by the endwalls. Owing to the computational cost, this represents a severe limitation which is not encountered in laboratory experiments. Because of this constraint and based on the experimental evolution of the front position displayed in Fig. 3, which reveals that the front velocity slowly decreases in time during a fairly long, transitional stage to reach a constant value, we expect the long-time front velocities obtained in the "short" tube computations to be slightly larger than their experimental counterparts, which were obtained after a much longer observation time. We stress again that the sole effect of the finite tube length during the stages of the flow considered in this paper is to impose a maximum observation time for the constant velocity regime without influencing any of the characteristics of the flow during this regime. The major characteristics of the mixing dynamics, especially the influence of the tilt angle on the evolution of the mixing zone, should be captured with this short numerical domain, provided the computed flow has reached the late stage corresponding to a balance between gravitational and inertial effects.

The computed front velocities normalized by the characteristic velocity V_t are plotted against the tilt angle θ in Fig. 4; the experimental results contained in Fig. 4 of Ref. 3 are also replotted for comparison. In both cases, the front veloci-

Downloaded 11 Feb 2011 to 194.167.203.33. Redistribution subject to AIP license or copyright; see http://pof.aip.org/about/rights_and_permissions

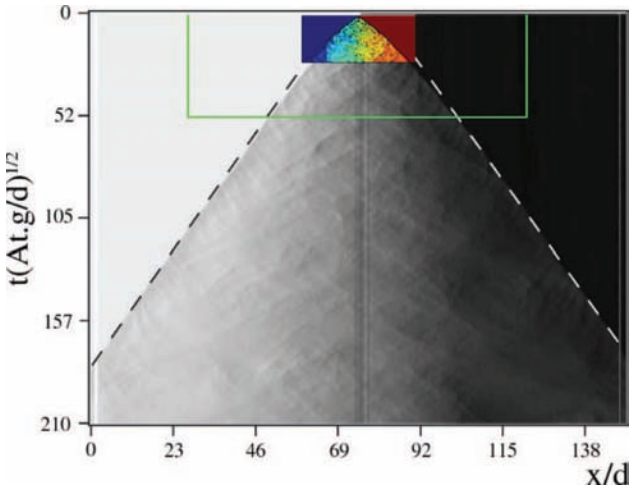

FIG. 3. (Color online) Spatiotemporal diagram of the front position in a cylindrical tube with $\theta=30°$. In grayscale: Experimental diagram obtained by Séon (Ref. 2). In color scale $[t(\mathrm{At}g/d)^{1/2}<20]$ (online): Computational diagram. The rectangle corresponding to $t(\mathrm{At}g/d)^{1/2}<52$ marks the final stage reached in the extended parallel computation.

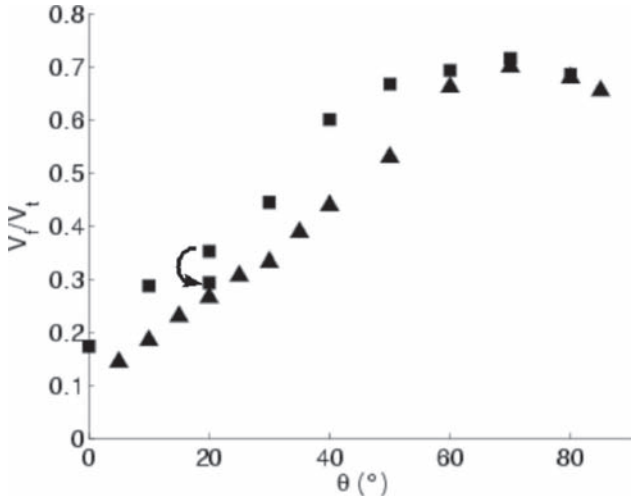

FIG. 4. Computational (■) and experimental (▲) values of the normalized front velocities in a tilted cylindrical tube. The final dimensionless time $T=t(\mathrm{At}g/d)^{1/2}$ ranges from 18 to 42 in the simulations, while it is about 200 in the experiments. The arrow points toward the value of V_f/V_t obtained from the extended parallel simulation for which $T\approx 54$.

ties are computed from the local slope of the boundary of the mixing zone, i.e., from the dashed line separating pure fluid regions from the mixing zone in Fig. 3 (throughout this paper, we define the mixing zone as the flow region where $0.01<C<0.99$ and determine the front velocity from spatiotemporal diagrams similar to that of Fig. 3, unless specified otherwise). As expected from the Introduction, three well distinct regimes may be readily identified. A clear plateau is found for tilt angles between 55° and 80°, whereas the expected viscous decrease of the front velocity is observed for higher angles. For values of θ less than 55°, the inertial increase of the front velocity with the tilt angle is recovered and the corresponding slope is close to that determined in the experiments. The maximum velocity of the front V_p reached for $\theta=70°$ is found to be $0.717V_t$, whereas a value of $0.703V_t$ was reported in the experiments. The difference is about 2%, which is the order of magnitude of the experimental accuracy.

Finally, to make sure that longer computations in longer tubes would allow us to obtain front velocities in close agreement with the experiments, we ran an extra simulation in a $96d$ long tube with a tilt angle of 20°. For this purpose, we made use of a parallel version of the code with 1534 grid cells in the axial direction. The corresponding value of V_f is marked with an arrow in Fig. 4. It lies very close to the experimental value, indicating a close agreement between computations and experiments when the computational time is long enough.

To conclude, the various features displayed by the computational results obtained over the full range of tilt angles are in good agreement with the experimental findings. Even the quantitative differences observed on the values of the front velocity can be removed by running longer computations. Therefore, we are confident that our code allows us to perform "numerical experiments" on the large-scale concentration and velocity fields generated by the gravitational mixing.

In the following sections, we will also describe 2D simulations as well as 3D simulations in square channels. The 2D simulations are performed in a $d\times 64d$ domain discretized with 64×1024 cells. The dimensions of the square channels are $\sqrt{\pi}d/2\times\sqrt{\pi}d/2\times 32d$, so that they have the same cross-sectional area as the cylindrical tube described above. A $46\times 46\times 512$ grid is used to discretize them. The above choices allow us to describe all three geometries considered below with approximately identical resolutions.

IV. GLOBAL CHARACTERISTICS OF THE INITIAL SLUMPING PHASE

A. Horizontal channels

We begin with results concerning the front velocity observed during the initial slumping phase. This front velocity is known to remain approximately constant as long as viscous effects remain small. We first ran a simulation in a cylindrical tube at a Reynolds number $\mathrm{Re}=790$, identical to that used in the experiments of Refs. 1–4. The corresponding Froude number $F_d=V_f/\sqrt{g'd}$ was found to be 0.41, which is in close agreement with the experimental value $F_d=0.404$. In the same configuration, Benjamin's[21] theoretical prediction for an energy-conserving current is $F_d=0.542$. Therefore, it turns out that at the present Reynolds number of 790, the Froude number is only about 75% of the asymptotic value corresponding to an infinite Reynolds number. In the purely 2D case with the same Reynolds number (d now being the channel height), the computational results yield $F_d=0.37$, which is also only about 74% of Benjamin's well-known prediction $F_d=1/2$. Results obtained in a 3D square channel by keeping the fluid viscosity and the cross-sectional area identical to those of the above cylindrical tube computation (which results in $\mathrm{Re}=660$) yield a similar value $F_d=0.36$, indicating that 3D effects resulting from instabilities in the bulk of the current are negligible at this stage of the flow, in

Downloaded 11 Feb 2011 to 194.167.203.33. Redistribution subject to AIP license or copyright; see http://pof.aip.org/about/rights_and_permissions

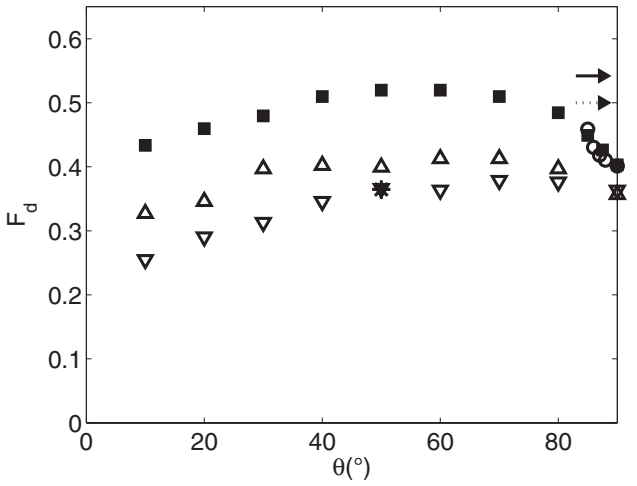

FIG. 5. Froude number during the initial slumping phase in a tilted tube for different geometries. Cylindrical tube (Re=790); (△) square channel (Re=660); (∗) 3D periodic channel (Re=660); (▽) 2D channel (Re=790); (○) experimental results in a cylindrical tube (Re=790) (Ref. 3); (—▶) and (···▶) inviscid prediction in a horizontal cylinder (0.542) and a horizontal 2D current (0.5), respectively (Ref. 21).

line with recent findings.[12,13] These values of the Froude number demonstrate that viscous dissipation is significant at moderate Reynolds numbers (in particular in the present range $5\times10^2<\mathrm{Re}<10^3$), even during the initial stages of the flow. Moreover, the results found for the cylindrical and square channels indicate that these viscous processes have an almost identical strength in both geometries.

The results corresponding to the two types of square channels, i.e., with either lateral walls or periodic boundary conditions in the spanwise direction, provide other interesting indications. Indeed, we found $F_d=0.36$ in both cases, even though stronger near-wall viscous effects can be expected in the square duct, as compared to the periodic 3D channel, due to the two additional boundary layers. This means that even though viscosity plays a role at such moderate Reynolds numbers, wall friction effects on lateral walls are negligibly small.

B. Tilted channels

The Froude number measured during the initial slumping phase of inclined currents is plotted in Fig. 5. Some experimental determinations of F_d by Séon[2] for nearly horizontal cylindrical tubes are also reported in this figure; the corresponding simulations reveal an excellent agreement with these experiments. For intermediate tilt angles, the Froude number is observed to gradually increase with the angle in all four geometries. Then, a plateau region takes place until F_d decreases with θ when the tube is close to horizontal. This decrease is found to be especially strong in the cylindrical geometry. It is worth noting that these significant, although mild, variations of F_d with θ contrast with the well-established independency of the front velocity with respect to the slope in unconfined gravity currents over an inclined plane.[10] Therefore, the angular dependence displayed in Fig. 5 is a clear mark of the constraints put on the flow development by the geometrical confinement, especially by the presence of the top wall. The obvious reason for this change is that no net flow can take place in the confined configurations considered here, so that the ascending and descending currents carry the same flow rate. Hence, the vertical extent of the head of the descending current is constrained by the ascending counterflow, which is in contrast with the classical unconfined situation where the lack of vertical confinement allows the height of the head above the incline and, consequently, the entrainment inside it, to increase with the slope, thus limiting the front velocity.

Turning to the differences between the four geometries considered in Fig. 5, we first notice that the front velocity in a cylindrical tube is larger than that in both 2D channels and 3D square channels at any tilt angle. From the simulation performed in a periodic 3D channel at $\theta=50°$, we also find an indication that the slumping phase is essentially 2D, even in tilted tubes, when the geometry does not impose any specific three-dimensionality of the flow (in this geometry, the spanwise symmetry is eventually broken near the end of the slumping phase, due to numerical truncation errors). In contrast, the front velocity in 2D currents is observed to be lower than that measured in a square channel for any nonzero tilt angle, even though the Reynolds number of the former is slightly larger than that of the latter. While this difference seems surprising at first glance, it may be explained by the following argument. Lateral walls promote 3D effects which quickly break the initial 2D coherent structures, whereas these structures obviously persist in a 2D flow. As will be discussed in the next section, 3D vortical structures enable larger front velocities than 2D vortices, so that the observed difference is in line with this general trend. Finally, Fig. 5 reveals that F_d is roughly constant over a wide range of tilt angles, say, between 40° and 70°–80°. Birman *et al.*[8] observed a qualitatively similar dependency on θ in a 2D flow with Re=4000 and $\rho_1/\rho_2=0.998$ but measured higher front velocities, namely, $F_d\simeq0.48$ for $\theta=90°$ and $F_{d\,\max}\simeq0.59$ for $\theta=50°$. The difference between present results and those of Ref. 8 has two origins, keeping in mind that Fig. 1 indicates that both codes give very similar results when using identical boundary conditions and identical values of Re and At (other tests, not reported here, show that this agreement also holds for tilted geometries). First, the Reynolds number used in the present computations is about five time smaller than that of Ref. 8, so that part of the aforementioned differences is due to the significant dependency of F_d on the Reynolds number in the moderate-Re range. Then, Ref. 8 made use of free-slip boundary conditions, whereas no-slip conditions are prescribed in the present simulations, increasing viscous dissipation and thus decreasing F_d. The same authors performed experiments at $\mathrm{At}=6\times10^{-3}$ and Re=1250 in a cylindrical tube. They observed a broad maximum $F_{d\,\max}$ of the Froude number about 0.53 for a tilt angle $\theta_{\max}$ around 75°. Figure 5 shows a very close computational value of $F_{d\,\max}$ but the corresponding value of $\theta_{\max}$ is about 55°. Interestingly, this value of $\theta_{\max}$ is exactly that corresponding to the maximum rising speed of long gas bubbles in inclined tubes,[22] but this agreement has to be taken with caution since the value of $\theta_{\max}$ probably depends on Re.

Downloaded 11 Feb 2011 to 194.167.203.33. Redistribution subject to AIP license or copyright; see http://pof.aip.org/about/rights_and_permissions

FIG. 6. Snapshots of the concentration (top) and swirling strength (bottom) in three different geometries at two contrasted tilt angles (the views are taken in the vertical or central plane of the tube/channel).

V. LONG-TIME BEHAVIOR

At the end of the slumping phase, viscous effects enter into play and the front velocity starts decreasing in time (see the time record of the front velocity in Fig. 8). This marks the beginning of the long-time behavior of the flow. Figure 6 (top) shows typical snapshots of the concentration field in a cylindrical tube, a square channel, and a 2D channel, respectively, for two widely contrasted tilt angles during this late stage. The corresponding swirling strength Λ, which may be thought of as an indicator of the instantaneous vorticity, is shown on the bottom of each figure (Λ is defined as the imaginary part of the conjugate eigenvalues of the velocity gradient tensor, see Refs. 23 and 24 for a comparison of the various vortex identification schemes).

In 3D flows, when the tilt angle lies approximately between 60° and 80° [Figs. 6(a) and 6(b)], the vortices resulting from the Kelvin–Helmholtz instability generated by the shear between the ascending and descending currents are not strong enough to cut, even temporarily, the channel of pure light (heavy) fluid that rises along the upper (lower) wall. Therefore, in this regime, the concentration jump across the front of the heavy current is $C_f=1$ (keep in mind that $C=0$ in the pure light fluid) and the front velocity is independent of θ with $V_f=0.7V_t$ in the cylindrical geometry, as shown in Sec. III. In contrast, for lower tilt angles [Figs. 6(d) and 6(e)], the shear overwhelms the segregational effects produced by the transverse gravity component ($g\sin\theta$) and the Kelvin–Helmholtz rolls are strong enough to temporarily cut these channels of pure fluid. The concentration in the head of the light (heavy) current then results from an equilibrium between the local mixing and the feeding by the pure fluid located upstream (downstream) near the upper (lower) wall. If the channel of pure fluid is cut by vortices, the local mixing makes C_f decrease, imposing a decrease in the front velocity. Then, the vortices that broke the channel of incoming fluid stretch and break, enabling some pure fluid to reach the head again, which leads to a reincrease of C_f. As a result, this regime is characterized by time variations of C_f. The mean value of C_f, which determines V_f, thus depends on the intensity and spatiotemporal organization of the vortices compared to the segregational effects of the transverse component of gravity, these various parameters all being controlled by the tilt angle θ. Séon *et al.*[3] noticed that in this regime, the normalized front velocity V_f/V_p in a cylindrical tube scales as $\sqrt{C_f}$. We computationally evaluated C_f in a cylindrical tube and a 2D channel by performing a volume average of C

Downloaded 11 Feb 2011 to 194.167.203.33. Redistribution subject to AIP license or copyright; see http://pof.aip.org/about/rights_and_permissions

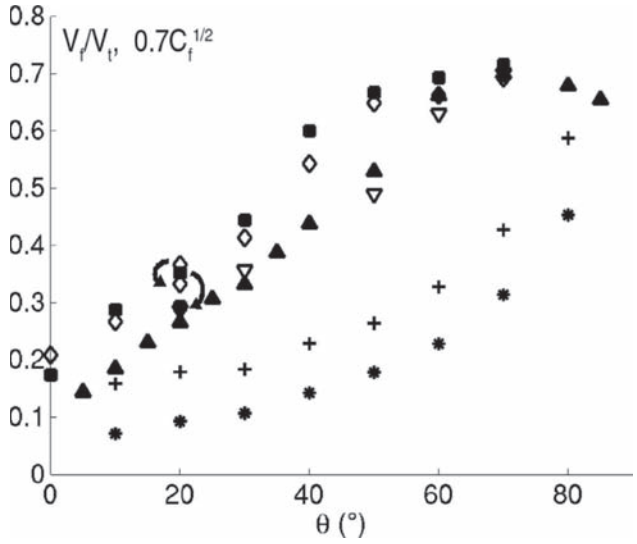

FIG. 7. Computational and experimental values of the normalized front velocities (V_f/V_t) and density contrast ($0.7\sqrt{C_f}$) in cylindrical and 2D tilted tubes. ■ (◇), Computational values of V_f/V_t ($0.7\sqrt{C_f}$) in a cylindrical tube; ▲ (▽), experimental (Ref. 3) values of V_f/V_t ($0.7\sqrt{C_f}$) in a cylindrical tube; * (+), V_f/V_t ($0.7\sqrt{C_f}$) obtained in 2D computations. The arrows point toward the values of V_f/V_t and $0.7\sqrt{C_f}$ obtained in the extended parallel simulation at a dimensionless time $T\approx 54$.

over a $0.25d$ long volume in the head of the heavy stream. The corresponding values of $\sqrt{C_f}$, together with those of V_f/V_t recorded at a dimensionless time $T\approx 20$, are reported in Fig. 7 (due to the computational time limitation discussed in Sec. III, these values are generally slightly larger than those determined experimentally[3]). Indeed, in the cylindrical geometry, the normalized front velocity is found to be directly proportional to $\sqrt{C_f}$ over the whole range of angles $\theta < 80°$. Keeping in mind that $V_f=0.7V_t$ when $C_f=1$, the computations indicate $V_f\approx 0.7V_t\sqrt{C_f}$, which is the experimental law obtained in Ref. 3.

In 2D situations, the Kelvin–Helmholtz vortices are much more coherent than their 3D counterpart, enabling them to reach higher intensities and to live longer. Thanks to this long lifetime, a chain of vortices can easily develop inside the body of the current, blocking efficiently the feeding of the fronts. This phenomenon is easily discernible in Fig. 6(c) in the case $\theta=60°$ where a chain of vortices has developed within the body of the mixing region and is about to break the channels of pure fluid. The same phenomenon was observed for any value of θ in the 2D simulations, leading us to conclude that the channels of pure fluid can be broken at any tilt angle in this geometry. In direct connection with this trend, C_f was found to slowly decrease after a short period of time, imposing a related decrease to the front velocity. No intermediate regime with $C_f=1$ was detected, explaining why no plateau is found for 2D flows in Fig. 7. However, it may be noticed from this figure that while V_f remains linked to $\sqrt{C_f}$, the relation $V_f/V_t=0.7\sqrt{C_f}$ does not hold anymore. Rather, the relation that emerges from Fig. 6 is of the type $V_f/V_t=0.7\sqrt{C_f}+\beta$. We also note from Fig. 6 that the front velocity is smaller at any tilt angle in two dimensions than in three dimensions, the difference being especially large for $40° < \theta < 75°$. This is a direct consequence of the absence of persistent pure fluid channels in the 2D configuration.

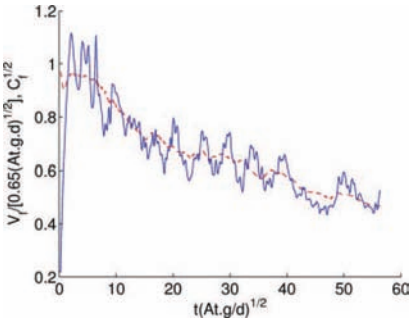

FIG. 8. (Color online) Time record of the front velocity (solid line) and square root of the relative concentration jump across the front (dashed line) for a cylindrical tube with $\theta=20°$.

VI. SOME SALIENT FEATURES OF THE FLOW DYNAMICS

We previously insisted on the direct connection between the pseudostationary front velocity V_f and the front density contrast C_f in the long-time regime. The instantaneous values of V_f and $\sqrt{C_f}$ are plotted in Fig. 8 in the case of a cylindrical tube inclined at 20°. Note that in order to observe transient effects, these values of V_f were obtained through a time differentiation of the successive positions of the front defined as $C=0.01$, not from the slope of the mixing region in a spatiotemporal diagram similar to that of Fig. 3, which implicitly filters out "rapid" fluctuations.

It may be observed that the long-time (i.e., low-frequency) evolution of V_f indeed follows that of $\sqrt{C_f}$. In contrast, it is clear that the front velocity evolution displays strong rapid variations that are not linked to the smooth evolution of the density contrast at the front. The frequency f of these fluctuations is such that $fd/V_t\simeq 0.16$. In order to clarify the origin of these short-time velocity fluctuations, we examined two indicators capable of shedding some light on the nature and topology of the flow in the front region. One of them is the volume fraction α filled by the head of the current (we identify the heavy current as the region of the flow where $C\geq 0.01$), while the other is the dimensionless swirling strength $\Lambda\sqrt{d/(Atg)}$ defined previously. Both indicators are computed through a volume average over a portion of the tube bounded by the cross section intersecting the front position and that located one diameter upstream.

Figure 9 presents a zoom of Fig. 8 over the time interval $20\leqslant T\leqslant 45$, with the addition of the aforementioned two indicators. It can easily be noted that the local maxima of V_f correspond to the local minima of α and Λ. This indicates that the volume of the head of the current and the front velocity are both correlated with the vortical activity within the head. Figure 9 reveals that the deceleration periods simultaneously occur with the growth of the head. An increase of the size of the head with a constant-density difference would lead to an increased buoyancy force that should make the front accelerate. Since this does not occur, we have to

Downloaded 11 Feb 2011 to 194.167.203.33. Redistribution subject to AIP license or copyright; see http://pof.aip.org/about/rights_and_permissions

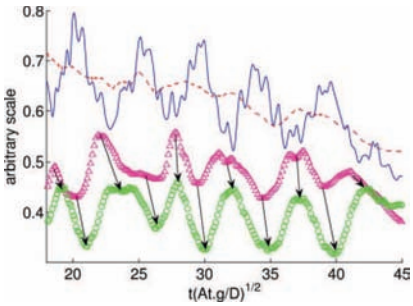

FIG. 9. (Color online) Time record of $V_f/(0.65\sqrt{\mathrm{At}gd})$ (solid line), $C_f^{1/2}$ (dashed line), α (○), and $\Lambda[d/(\mathrm{At}g)]^{1/2}$ (△) for a cylindrical tube with $\theta=20°$. The various curves have been arbitrarily translated in the vertical direction.

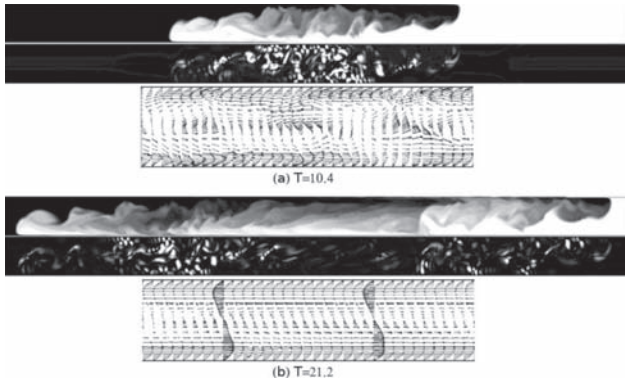

FIG. 10. Two stages of the evolution of the concentration (top), swirling strength (center), and velocity (bottom) in a cylindrical tube with $\theta=60°$ (the views are taken in the vertical diametrical plane of the tube). (a) The middle of the tube is filled with a highly vortical flow ($T=10.4$); (b) birth of a two-layer flow region with virtually no vorticity in the middle of the tube ($T=21.2$).

conclude that the front deceleration is due to the increase in the vortical activity that simultaneously takes place. The growth of the corresponding vortex yields that of the head volume, which leads to a local increase of the potential energy available in the head. Then, the vortical structure is advected in the mixing zone (leading to a decrease of Λ) and the new amount of potential energy in the head is converted back into kinetic energy (making α decrease), thanks to a slumping of the head, which leads to a reincrease of the front velocity. As shown in Fig. 9, this cycle repeats itself a number of times. A similar behavior, where vortex interactions are responsible for an increase of the potential energy in the head, yielding fluctuations of the front velocity, was recently reported for horizontal gravity currents.[12] However, the phenomenon was found to be fairly sporadic, whereas we find it to be present all along the long-time evolution in confined geometries. The above observations lead us to conclude that time variations of C_f impose low-frequency variations of V_f, while interactions between the vorticity field and the current head can be responsible for high-frequency fluctuations of the front velocity.

The plot of the swirling strength highlights another interesting feature. While the Λ-fields look almost "turbulent" with a good degree of local mixing in 3D configurations, the vortices are well defined and bounded in the 2D channel [Figs. 6(c) and 6(f)]. In the latter case, the flow inside the mixing zone is clearly organized in cells whose characteristic size is the diameter of the channel. Although this spatial organization is not permanent, this vortex chain can persist during sufficiently long times to tear off the head of the current and definitely separate it from the mixing zone [this phenomenon is about to happen in Fig. 6(c)]. The head then behaves as a "bubble" of light fluid (or a "drop" of heavy fluid) and is subsequently slowly destroyed by diffusion or wrenching in its own wake. We observed temporary separations of the front in 2D channels for tilt angles less than 80°, while the phenomenon was found to occur only for θ less than 40° in the square duct and the 3D periodic channel. However, in contrast with the 2D case where reconnection of the front may not occur after it has been separated from the mixing region, reconnection always occurred after some time in the above two 3D configurations. Moreover, we never observed any separation sequence in cylindrical tubes, which suggests that among the configurations considered here, this is the one in which vortices have the weakest coherence.

Figure 10(a) shows a stage of the flow in a cylindrical tube during which the central region is quite well mixed and only little pure fluid is feeding the fronts, thanks to a strong vortical activity. We previously mentioned that such a spatial organization is not permanent in the 2D case and the same turns out to be true in 3D situations. Indeed, in Fig. 10(b) which corresponds to a later stage, we notice the occurrence of a two-layer flow structure. The corresponding snapshot of the swirling strength indicates that the vorticity is very low throughout this region. This succession of two contrasted states is reminiscent of observations of intermittency reported by Séon *et al.*[4] These authors noticed that a mixed state in which the density is fairly constant within a cross section but exhibits a gradient along the tube axis [as in Fig. 10(a)] can be destabilized to give birth to a two-layer flow [as in Fig. 10(b)], which in turn can be affected by a Kelvin–Helmholtz instability, the effect of which is to reset the initial mixed configuration. They also pointed out that the mixing efficiency is strongly increased during the relaxation to the initial mixed state. Unfortunately, we could not observe the last part of such a cycle numerically because its period is of the same order as that required for the two currents to reach the extremities of the computational domain. The extended parallel simulations should allow us to remove this limitation.

VII. SUMMARY AND CONCLUSIONS

The present computations shed light on several important effects of channel geometry on the gravitational mixing of two miscible fluids placed in an inclined channel or tube. During the initial slumping phase, the results obtained in a periodic 3D channel confirm that the current dynamics are essentially 2D. They indicate that the current in a 3D square channel is faster that its unconfined counterpart at any nonzero tilt angle, so that 2D models would fail to predict the correct front velocity in the former case. As expected from inviscid theory, currents are significantly faster in cylindrical

Downloaded 11 Feb 2011 to 194.167.203.33. Redistribution subject to AIP license or copyright; see http://pof.aip.org/about/rights_and_permissions

tubes than in any rectangular geometry. A common feature observed in all geometries in this early stage is that the front velocity is roughly constant in an intermediate range of tilt angles (with the values of At and Re considered in the present computations, this range was found to be approximately $40° < \theta < 75°$) and slightly decreases in nearly vertical and nearly horizontal configurations. In later stages, the front velocity at a given tilt angle is always smaller in 2D flows than in 3D configurations. More importantly, the three regimes found in 3D flows at small, intermediate, and large tilt angles have no counterpart in two dimensions. This may be understood by examining the concentration jump across the front in connection with the structure of the vortical motions. While $C_f = 1$ in 3D flows for $55° < \theta < 80°$ because the fronts are fed with pure fluid due to the moderate strength of the vortices, the latter are much more intense and coherent in two dimensions. Therefore they are able to cut the pure fluid channels at any tilt angle, thus lowering C_f. We also observed that these intense 2D vortices are able to tear off the head of the current and definitively separate it from the body of the current. In contrast, such separations are only temporary in 3D rectangular channels and never occur in a cylindrical tube. Finally, despite the limited physical time reached in most of the computations performed in a cylindrical tube, the results fully confirm the experimental finding of Ref. 3 concerning the relation between the time-averaged velocity and the concentration jump at the front, namely, $V_f \approx 0.7 V_t \sqrt{C_f}$. In two dimensions, the computational results indicate that V_f is still connected to $\sqrt{C_f}$ over the whole range of tilt angles but the absence of any plateau in the variation of V_f with θ prevents this relation to be reduced to the above form, a point which will deserve further investigation. In contrast, the short-time, i.e., high-frequency, evolution of V_f is not connected to that of C_f. Rather, our results show that it is directly related to the local vortical activity in the head which, by a succession of hydrodynamic mechanisms, converts potential energy into vortical energy and vice versa.

The results reported here show that direct numerical simulation is a powerful and reliable tool to investigate the complex dynamics of this class of flow. It appears to be very complementary to laboratory experiments, especially in order to elucidate the connection between the evolution of the concentration field and that of the complex vortical structure of the flow. In the next step of our work, we plan to explore in detail several aspects of this connection.

ACKNOWLEDGMENTS

We warmly thank Annaig Pedrono for her continuous and decisive support in the development of the code, especially the parallel version, and Jean-Pierre Hulin and Thomas Bonometti for fruitful discussions and careful reading of the manuscript. The support of the CINES in Montpellier, which provided part of the CPU time, was greatly appreciated.

[1] T. Séon, J. P. Hulin, D. Salin, B. Perrin, and E. J. Hinch, "Buoyancy driven miscible front dynamics in tilted tubes," Phys. Fluids **17**, 031702 (2005).
[2] T. Séon, "Du mélange turbulent aux courants de gravité en géométrie confinée," Ph.D. thesis, University Paris XI, 2006.
[3] T. Séon, J. P. Hulin, D. Salin, B. Perrin, and E. J. Hinch, "Laser-induced fluorescence measurements of buoyancy driven mixing in tilted tubes," Phys. Fluids **18**, 041701 (2006).
[4] T. Séon, J. Znaien, B. Perrin, E. J. Hinch, D. Salin, and J. P. Hulin, "Front dynamics and macroscopic diffusion in buoyant mixing in a tilted tube," Phys. Fluids **19**, 125105 (2007).
[5] D. I. H. Barr, "Densimetric exchange flows in rectangular channels," Houille Blanche **22**, 619 (1967).
[6] J. O. Shin, S. B. Dalziel, and P. F. Linden, "Gravity currents produced by lock exchange," J. Fluid Mech. **521**, 1 (2004).
[7] V. K. Birman, J. E. Martin, and E. Meiburg, "The non-Boussinesq lock-exchange problem. Part 2. High-resolution simulations," J. Fluid Mech. **537**, 125 (2005).
[8] V. K. Birman, B. A. Battandier, E. Meiburg, and P. F. Linden, "Lock-exchange flows in sloping channels," J. Fluid Mech. **577**, 53 (2007).
[9] G. H. Keulegan, "The motion of saline fronts in still water," National Bureau of Standards Report, 1958.
[10] R. E. Britter and P. F. Linden, "The motion of the front of a gravity current travelling down an incline," J. Fluid Mech. **99**, 531 (1980).
[11] C. Härtel, E. Meiburg, and F. Necker, "Analysis and direct numerical simulation of the flow at a gravity-current head. Part 1. Flow topology and front speed for slip and no-slip boundaries," J. Fluid Mech. **418**, 189 (2000).
[12] M. I. Cantero, J. R. Lee, S. Balachandar, and M. H. Garcia, "On the front velocity of density currents," J. Fluid Mech. **586**, 1 (2007).
[13] F. Necker, C. Härtel, L. Kleiser, and E. Meiburg, "High-resolution simulations of particle-driven gravity currents," Int. J. Multiphase Flow **28**, 279 (2002).
[14] F. Necker, C. Härtel, L. Kleiser, and E. Meiburg, "Mixing and dissipation in particle-driven gravity currents," J. Fluid Mech. **545**, 339 (2005).
[15] T. Ellison and J. Turner, "Turbulent entrainment in a stratified flow," J. Fluid Mech. **6**, 423 (1959).
[16] A. N. Ross, P. F. Linden, and S. B. Dalziel, "A study of three-dimensional gravity currents on a uniform slope," J. Fluid Mech. **453**, 239 (2002).
[17] A. W. Cook and P. E. Dimotakis, "Transition stages of Rayleigh-Taylor instability between miscible fluids," J. Fluid Mech. **443**, 69 (2001).
[18] I. Calmet and J. Magnaudet, "Large eddy simulation of high-Schmidt-number mass transfer in a turbulent channel flow," Phys. Fluids **9**, 438 (1997).
[19] S. T. Zalesak, "Fully multidimensional flux-corrected transport algorithms for fluids," J. Comput. Phys. **31**, 335 (1979).
[20] J. Magnaudet and G. Mougin, "Wake instability of a fixed spheroidal bubble," J. Fluid Mech. **572**, 311 (2007).
[21] T. B. Benjamin, "Gravity currents and related phenomena," J. Fluid Mech. **31**, 209 (1968).
[22] E. E. Zukoski, "Influence of viscosity, surface tension, and inclination angle on motion of long bubbles in closed tubes," J. Fluid Mech. **25**, 821 (1966).
[23] J. Zhou, R. J. Adrian, S. Balachandar, and T. M. Kendall, "Mechanisms for generating coherent packets of hairpin vortices in channel flow," J. Fluid Mech. **387**, 353 (1999).
[24] P. Chakraborty, S. Balachandar, and R. J. Adrian, "On the relationships between local vortex identification schemes," J. Fluid Mech. **535**, 189 (2005).

Downloaded 11 Feb 2011 to 194.167.203.33. Redistribution subject to AIP license or copyright; see http://pof.aip.org/about/rights_and_permissions